A new ice cloud parameterization for infrared radiative transfer simulation of cloudy radiances: Evaluation and optimization with IIR observations and ice cloud profile retrieval products

Jerome Vidot, Anthony Baran, Pascal Brunel

▶ **To cite this version:**

Jerome Vidot, Anthony Baran, Pascal Brunel. A new ice cloud parameterization for infrared radiative transfer simulation of cloudy radiances: Evaluation and optimization with IIR observations and ice cloud profile retrieval products. Journal of Geophysical Research: Atmospheres, 2015, 120 (14), pp.6937-6951. ⟨10.1002/2015JD023462⟩. ⟨hal-03496972⟩

HAL Id: hal-03496972

https://hal.science/hal-03496972v1

Submitted on 21 Dec 2021

HAL is a multi-disciplinary open access archive for the deposit and dissemination of scientific research documents, whether they are published or not. The documents may come from teaching and research institutions in France or abroad, or from public or private research centers.

L'archive ouverte pluridisciplinaire **HAL**, est destinée au dépôt et à la diffusion de documents scientifiques de niveau recherche, publiés ou non, émanant des établissements d'enseignement et de recherche français ou étrangers, des laboratoires publics ou privés.

Copyright - All rights reserved

AGU PUBLICATIONS

JGR

Journal of Geophysical Research: Atmospheres

RESEARCH ARTICLE
10.1002/2015JD023462

Key Points:
- A new ice cloud parameterization for infrared fast RTM is proposed
- It does not need information about the size and the shape of ice particles
- Validation with ice cloud profile retrieval products is conducted

Correspondence to:
J. Vidot,
jerome.vidot@meteo.fr

Citation:
Vidot, J., A. J. Baran, and P. Brunel (2015), A new ice cloud parameterization for infrared radiative transfer simulation of cloudy radiances: Evaluation and optimization with IIR observations and ice cloud profile retrieval products, *J. Geophys. Res. Atmos.*, *120*, 6937–6951, doi:10.1002/2015JD023462.

Received 2 APR 2015
Accepted 28 JUN 2015
Accepted article online 1 JUL 2015
Published online 21 JUL 2015

©2015. American Geophysical Union. All Rights Reserved.

A new ice cloud parameterization for infrared radiative transfer simulation of cloudy radiances: Evaluation and optimization with IIR observations and ice cloud profile retrieval products

Jérôme Vidot[1], Anthony J. Baran[2], and Pascal Brunel[1]

[1]Centre de Météorologie Spatiale, DP/Météo-France, Lannion, France, [2]Met Office, Exeter, UK

Abstract A new ice cloud optical property database in the thermal infrared has been parameterized for the RTTOV radiative transfer model. The Self-Consistent Scattering Model (SCSM) database is based on an ensemble model of ice crystals and a parameterization of the particle size distribution. This convolution can predict the radiative properties of cirrus without the need of a priori information on the ice particle shape and an estimate of the ice crystal effective dimension. The ice cloud optical properties are estimated through linear parameterizations of ambient temperature and ice water content. We evaluate the new parameterization against existing parameterizations used in RTTOV. We compare infrared observations from Imaging Infrared Radiometer, on board CALIPSO, against RTTOV simulations of the observations. The simulations are performed using two different products of ice cloud profiles, retrieved from the synergy between space-based radar and lidar observations. These are the 2C-ICE and DARDAR products. We optimized the parameterization by testing different SCSM databases, derived from different shapes of the particle size distribution, and weighting the volume extinction coefficient of the ensemble model. By selecting a large global data set of ice cloud profiles of visible optical depths between 0.03 and 4, we found that the simulations, based on the optimized SCSM database parameterization, reproduces the observations with a mean bias of only 0.43 K and a standard deviation of 6.85 K. The optimized SCSM database parameterization can also be applied to any other radiative transfer model.

1. Introduction

The assimilation of infrared cloudy radiances from satellite observations is a major goal in improving numerical weather prediction (NWP) models [*Errico et al.*, 2007]. In the microwave spectral domain (10–100 GHz), the operational assimilation of satellite observations is already performed in all-weather conditions [*Bauer et al.*, 2011]. In the infrared spectral domain (3–20 μm), the assimilation of satellite observations is only performed in clear-sky and in overcast cloudy conditions [*Pavelin et al.*, 2008; *McNally*, 2009; *Guidard et al.*, 2011]. The limitation to overcast cloudy conditions is mainly due to the large nonlinear sensitivity of infrared radiances to cloud parameters of the simplified single-layer cloud model (cloud fraction and cloud top height) used in the operational assimilation of infrared radiances. Furthermore, the advantage of assimilating overcast cloudy radiances is to exclude the modeling of multiple scattering. However, fast radiative transfer models (RTMs) developed for the assimilation of satellite observations in NWP models are also able to simulate infrared radiances in more complex cloudy conditions. For that, they use NWP model cloud variables (ice and liquid water content profiles and cloud fraction profiles) as input information together with parameterization of cloud particle optical properties. This capability has shown encouraging results in improving assimilation of infrared cloudy radiances [*Stengel et al.*, 2010, 2013; *Martinet et al.*, 2013a; *Okamoto et al.*, 2013] using the radiative transfer model for TOVS (RTTOV) [*Saunders et al.*, 1999; *Matricardi et al.*, 2004]. This improvement has been achieved by more accurate modeling of cloud scattering and multilayer clouds.

A key step in better simulating infrared cloudy radiances for RTTOV is to improve the parameterization of cirrus optical properties from NWP model cloud variables. For ice cloud, the version 9 of RTTOV [*Saunders et al.*, 2009] provides eight different parameterizations. These parameterizations come from four different empirical relationships, which were derived from different cloud studies and were based on aircraft measurements located in different geographical areas [*Ou and Liou*, 1995; *Wyser*, 1998; *Boudala et al.*, 2002; *McFarquhar et al.*, 2003]. These parameterizations are named hereafter OL95, W98, B02, and MF03,

respectively. These empirical relationships relate the ice crystal effective diameter (D_{eff}) to the ice water content (IWC) and/or the ambient temperature (T). The ice cloud optical properties were then parameterized as functions of D_{eff} and IWC for two shapes of ice crystals, i.e., the randomly oriented hexagonal ice column and ice aggregate. A full description of the parameterizations can be found in *Matricardi* [2005] and in *Saunders et al*. [2009]. However, these previous parameterizations developed for RTTOV are based on particle size distributions (PSDs) which are highly likely to be biased toward smaller ice crystals due to ice crystal shattering on or at the inlets of microphysical probes [*Korolev et al*., 2011]. Additionally to these eight parameterizations, two more parameterizations were provided in an updated RTTOV version 10.2, which allows the user to input directly vertical profiles of D_{eff} to RTTOV for each assumed ice crystal shape [*Saunders et al*., 2012]. Hereafter, this parameterization is named DE.

The current problem with the RTTOV ice parameterizations is that users are provided with a wide choice of parameterizations which leads to difficulties in deciding which might be best for their particular application. For instance, simulations of one typical top-of-atmosphere (TOA) infrared brightness temperature (BT) spectra show few tens of kelvin's difference in window channels for the same ice cloud profile using the different parameterizations [*Faijan et al*., 2012; *Vidot et al*., 2013]. However, *Faijan et al*. [2012] show also that no parameterization globally provides a unique choice of parameterization when simulating many Infrared Atmospheric Sounding Interferometer (IASI) spectra in the presence of semitransparent clouds. Inversely, *Martinet et al*. [2013b] preferred the B02 parameterization, with randomly oriented hexagonal ice column crystals, for channel selection of the Infrared Atmospheric Sounding Interferometer (IASI) instrument in cloudy retrievals. In other studies, the W98 parameterization, which assumes aggregate ice crystals, was chosen [*Stengel et al*., 2013; *Okamoto et al*., 2013]. However, it is worth mentioning here that care must be taken with the aggregate shape of ice crystals from RTTOV, since it has been shown by simulated infrared spectra that the parameterization leads to unphysical spectral behavior between 10 and 12 μm [*Faijan et al*., 2012; *Vidot et al*., 2013].

In this study, we attempt to evaluate these ice cloud parameterizations together with a new parameterization provided in RTTOV version 11 [*Saunders et al*., 2013]. The new parameterization is based on a new database of bulk ice optical properties derived from the Self-Consistent Scattering Model (SCSM) for cirrus, called the ensemble model of ice crystals, and this model is fully described in the work of *Baran and Labonnote* [2007]. In this paper, we test a new SCSM bulk ice optical property database. This database combines the ensemble model of atmospheric ice particles with a particle size distribution (PSD) scheme that is consistent with microphysical observations, and this new SCSM optical property database is described in *Baran et al*. [2014a] and *Baran et al*. [2014b]. Alternative bulk ice optical property databases have been provided for the infrared spectral range [*Hess and Wiegner*, 1994; *Hess et al*., 1998; *Yang et al*., 2005; *Baum et al*., 2007; *Yang et al*., 2013; *Baum et al*., 2014, and references cited herein]. These databases were never incorporated into RTTOV, which is why they are not considered in this paper. We concentrate on RTTOV ice cloud parameterizations that are used in operational NWP centers. The novelty of this new parameterization is that the radiative properties of ice cloud can be predicted without the need for a priori information on the ice particle shape and an ice crystal effective diameter.

To compare and evaluate the RTTOV parameterizations, we used a large selection of products comprising of ice cloud profiles, retrieved from a combination of CloudSat [*Stephens et al*., 2002] and CALIPSO [*Winker et al*., 2009] observations. These ice cloud profiles are used to simulate infrared TOA BT. We then compare the simulations to the BT measured by the Imaging Infrared Radiometer (IIR) instrument, on board CALIPSO [*Garnier et al*., 2012], at 8.65, 10.6, and 12.05 μm. This comparison was motivated by two reasons: first, the better accuracy of ice cloud profiles retrieved by active sensors as compared to NWP outputs. Second, the fine spatial resolution of IIR (~1 km) allows the neglect of the effect of the vertical cloud fraction within a single pixel. Furthermore, this selection of ice cloud profiles and IIR BT observations was used to optimize the new ice cloud parameterization by modifying the calculation of the ice cloud optical property database by minimizing the difference between RTTOV simulations and IIR observations.

Section 2 of this article presents the new RTTOV-11 ice cloud parameterization and the modification of the SCSM database to optimize the new ice cloud parameterization. Section 3 is devoted to the selection of the ice cloud profiles, and the results are outlined in section 4. Conclusions and perspectives are given in section 5.

2. The RTTOV Ice Cloud Parameterization and the SCSM Databases

The infrared TOA BT of satellite-based observations in the presence of cloud is simulated by RTTOV using the Chou-scaling approximation [*Chou et al*., 1999]. The Chou-scaling approximation simplifies the cloud-scattering effect by estimating an effective extinction β_{eff}, at a wavelength λ of each cloud layer, given by

$$\beta_{\text{eff}}(\lambda, T, \text{IWC}) = \beta_{\text{abs}}(\lambda, T, \text{IWC}) + b(\lambda, T, \text{IWC})\beta_{\text{sca}}(\lambda, T, \text{IWC}), \quad (1)$$

where β_{abs} and β_{sca} are the volumetric absorption and scattering coefficients, respectively. The coefficient b is the backscattering fraction calculated from the phase function (see equation (32) of *Matricardi* [2005]).

In RTTOV-9, the ice cloud optical properties (β_{abs}, β_{sca}, and b) within each cloud layer are estimated from parameterization of IWC and D_{eff} profiles (see equations (35)–(37) of *Saunders et al*. [2009]) and where D_{eff} is parameterized as functions of T only (OL95) or IWC only (MF03) or T and IWC (W98 and B02).

In RTTOV-11 [*Saunders et al*., 2013], we have added a new parameterization of β_{abs}, β_{sca}, and b from T and IWC without the need of D_{eff}. The new parameterization is based on the Self-Consistent Scattering Model (SCSM) database of ice cloud optical properties. The SCSM database is based on the ensemble model of cirrus ice crystals shown in Figure 1 of *Baran and Labonnote* [2007]. The ensemble model consists of six habit members. The first habit is the hexagonal ice column of aspect ratio unity, where the aspect ratio is the quotient between the length and the diameter of the three-dimensional hexagon. The second habit is assumed to be the six-branched bullet rosette, followed by three-, five-, eight-, and ten-element hexagonal ice aggregates. For each of the hexagonal ice aggregates, the hexagonal monomers are arbitrarily attached to each other, forming compact and spatial ice aggregates. The orientation-averaged aspect ratio of each of these aggregate habits is given in Table 6 of *Baran and Labonnote* [2007]. To obtain the bulk-scattering optical properties, the ensemble model single-scattering properties were integrated over a moment estimation parameterization of the PSD due to *Field et al*. [2007], named hereafter F07. To generate the PSDs, a total number of 20,662 in situ estimates of IWC and in-cloud temperature measurements are applied to the F07 parameterization, given a mass-dimensional relationship. The PSD parameterization is further described below. The in situ estimates and measurements were obtained from a number of aircraft-based field campaigns located in the tropics and midlatitudes. The construction of the database used in this paper is fully described in *Baran et al*. [2011a] and *Baran et al*. [2014a] and so will not be repeated here. Each member of the ensemble can be assigned to a particular size bin. However, since the distribution of ensemble shapes throughout the PSD is unknown, the ensemble members are distributed into six equal intervals of the PSD, with the hexagonal columns being distributed into the first interval, and the last interval is occupied by the ten-element ice aggregate. The computation of the single-scattering SCSM optical property database is described in *Baran et al*. [2014a].

The F07 PSD parameterization is based on 10,000 in situ PSDs, which were filtered, by using particle interarrival times as described by *Field et al*. [2003] and *Field et al*. [2007], to reduce shattered ice artifacts distorting the shape of the small ice mode. Due to the shattering problem, the F07 parameterization ignored in situ measurements of ice crystal size less than 100 μm. To complete the PSD, the F07 parameterization assumes an exponential PSD to represent ice crystal size less than 100 μm, and this is added to a gamma function, for sizes greater than that. The F07 parameterization is shown to fit well to several cases of in situ measured-averaged PSDs obtained in the tropics [*Baran et al*., 2011a]. In the F07 parameterization, the second moment (i.e., the IWC) is linked to any other moment via polynomial fits to the in-cloud temperature. Thus, for any given IWC and in-cloud temperature, the original PSD can be estimated. It has been previously demonstrated by *Baran et al*. [2014a] that for several cases of ice cloud the SCSM bulk optical properties successfully simulated active and passive measurements from the UV to the microwave regions of the spectrum, while maintaining microphysical consistency across the spectrum.

The SCSM database consists of 20,662 PSDs (the compilation of the PSD database is described in *Baran et al*. [2014a]), that were generated from the F07 parameterization, using different in situ measured T and estimated IWC observations, and their distribution is shown in Figure 1. Figure 1 shows that the SCSM database covers a large range of both IWC and T values. The SCSM database provides for each PSD the simulated volumetric extinction and scattering coefficients and the asymmetry parameter at 145 wavelengths between 0.2 and 120 μm. In this paper, we utilize the database between 3 and 18 μm. The phase function is given by a linear

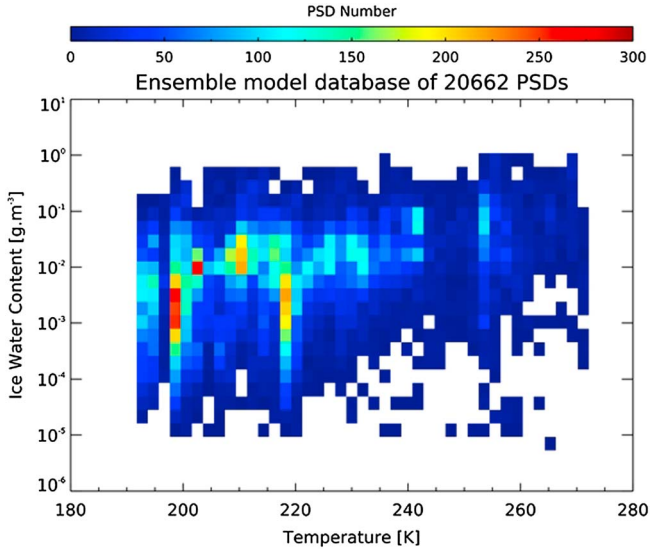

Figure 1. Two-dimensional histogram of ice water content (in g m^{-3}) versus temperature (in K) of the 20,662 PSD databases.

piecewise parameterization of the Henyey-Greenstein phase function, which depends only on the asymmetry parameter [*Baran et al.*, 2001], and is used to calculate the backscattering fraction coefficient b. The physical justification of using a phase function parameterization based on the Henyey-Greenstein phase function lies in the fact that in infrared range, the ice crystal phase function tends to be smooth in the backscattering region, with a strong diffraction peak in the forward scattering direction [*Yang et al.*, 2001]. The *Baran et al.*'s [2001] parameterization of the Henyey-Greenstein phase function has been shown to replicate short-wave multiangle satellite and aircraft observations of cirrus [*Baran et al.*, 2001; *Baran and Francis*, 2004] as well as high-resolution infrared observations of cirrus between 3.0 and 18.0 μm [*Baran and Francis*, 2004]. Therefore, for the purposes of this paper the *Baran et al.*'s [2001] parameterization of the Henyey-Greenstein phase function is sufficiently accurate.

It was found that the following equations gave the best fit to the distribution of bulk optical properties shown in Figure 1. The new parameterization has been implemented into RTTOV-11 and is given by the following equations:

$$\log_{10}[\beta_{\text{abs}}(\lambda,T,\text{IWC})] = A_a + B_aT + C_a\log_{10}(\text{IWC}) + D_aT^2, + E_a(\log_{10}(\text{IWC}))^2 + F_aT\log_{10}(\text{IWC}) \quad (2)$$

$$\log_{10}[\beta_{\text{sca}}(\lambda,T,\text{IWC})] = A_s + B_sT + C_s\log_{10}(\text{IWC}) + D_sT^2 + E_s(\log_{10}(\text{IWC}))^2 + F_sT\log_{10}(\text{IWC}), \quad (3)$$

$$b(\lambda,T,\text{IWC}) = A_b + B_bT + C_b\log_{10}(\text{IWC}). \quad (4)$$

The set of parameterization coefficients for β_{abs} (A_a to F_a), β_{sca} (A_s to F_s), and b (A_b to C_b) were calculated by using a nonlinear least squares fitting procedure over the SCSM database and are also functions of wavelength (omitted in equations for clarity). More details of this procedure can be found in *Saunders et al.* [2013].

It has been shown by *Baran et al.* [2011a] that the ensemble model predicts a mass-dimensional relationship of the form $m = aD^2$, where the prefactor a has a value of 0.04 and D is the maximum dimension of the ice crystal, where m and D are both in SI units [*Baran et al.*, 2011b]. This mass-dimensional relationship is applied to the F07 parameterization to generate the 20,662 PSDs, from which the bulk optical properties are obtained. We named, hereafter, this set of parameterization coefficients BV11. The BV11 parameterization was first improved by increasing the integration over the edges of the PSDs, leading to an improved SCSM database. An improved set of parameterization coefficients was then obtained, and this improved set is named B004. We tested new sets of parameterization coefficients afterward. This was achieved by changing the value of the prefactor and keeping the improvement of the integration over the PSD edges. In this paper, the values of the prefactor are assumed to be 0.015, 0.06, and 0.08. This range in prefactor value generates different shapes of the PSD. These new sets of parameterization coefficients are named hereafter B0.015, B0.06, and B0.08, respectively. A further SCSM database was also tested assuming a prefactor value of 0.0257, which corresponds to the value proposed by

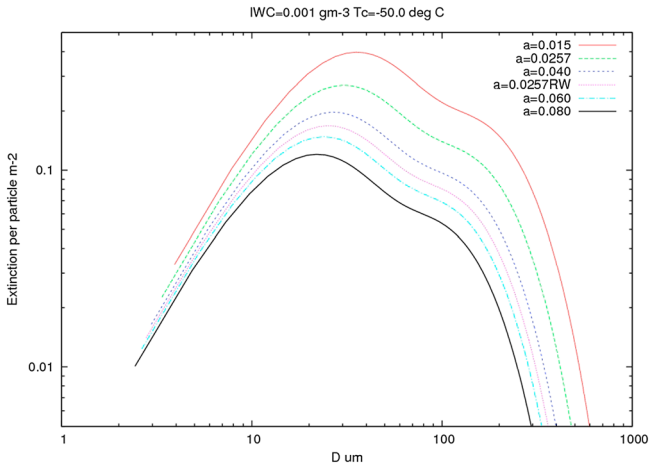

Figure 2. Extinction per particle in m^{-2} versus the maximum dimension of ice crystal D in μm for different values of the prefactor a of the mass-dimensional relationship throughout the exponent is set to a value of 2.0 (see text for explanation).

Cotton et al. [2013], and this other set of parameterization coefficients is named hereafter B0.0257. The use of this prefactor convolved with the F07 parameterization is microphysically consistent with the current cloud scheme used in the operational Met Office high-resolution NWP model [*Field et al.*, 2014]. We finally tested a last SCSM database, where the scattering and absorption coefficients of the B0.0257 database were scaled by a fixed value of 0.49, hereafter named B0.0257RW, where RW stands for reweighting. The motivation for reweighting the ensemble model is to obtain an SCSM database between those of parameterizations B0.04 and B0.06 while preserving the *Cotton et al.*'s [2013] observed values of the prefactor and exponent in the mass-dimensional relationship (i.e., $m = 0.0257\ D^2$). In this case, the weightings of the ensemble model volumetric extinction coefficient β_{ext} were achieved at each size bin of the PSD using the following equation:

$$\beta_{\text{ext}} = \int_{D_{\min}}^{D_{\max}} \left[\sum_{j=1}^{j=6} w_j \beta_{\text{ext},j}(D) \right] n(D) dD, \tag{5}$$

where $D_{\min}$ and $D_{\max}$ are the minimum and maximum values of the ice crystal maximum dimension in the F07 PSDs and w_j is the weight applied to each member of the ensemble model at each size bin. By definition, $\Sigma w_j = 1$ at each size bin. Finally, $n(D)$ is the ice crystal number concentration at each size bin predicted by the F07 PSD parameterization. To preserve the shape of the PSD using the constrain mass-dimensional relationship it was necessary to reweight the ensemble model using equation (5). If we assume the *Cotton et al.*'s [2013] observed microphysics (i.e., B0.0257) to be the best estimate of the mass-dimensional relationship, and applying this to the F07 parameterization, we will fix the underlying shape of the PSD. Given a fixed underlying shape of the PSD, the particle concentration per bin size can change, given the different profiles of IWC and T. Given the fixed underlying shape of the PSD, the ensemble model members were reweighted, such that the scattering and absorption coefficients were equivalent to the coefficients using a prefactor of between 0.04 and 0.06. This equivalence is achieved by using equation (5). The percentage contribution of each of the ensemble model members to the extinction coefficient (i.e., scattering plus absorption) per bin size was found to be 30% hexagonal columns; 30% six-branched bullet rosettes; and 10%, 20%, and finally 10% of three- to eight-branched ice aggregates, respectively. This idealized habit-weighted distribution may not represent the microphysical constitution of actual cirrus, but may simulate radiative equivalent cirrus, given a fixed underlying shape of the PSD.

The different prefactors were used to either broaden the F07 PSD or narrow the PSD to change the transmission properties of the cloud. The exponent of the mass-dimensional relationship was kept constant at a value of 2.0, as this value is consistent with the literature (see *Cotton et al.* [2013] for details and references therein). Figure 2 shows the extinction per particle versus the maximum dimension of ice crystal D for an assumed IWC value of 0.001 g m^{-3} and an assumed cloud temperature value of −50°C. The figure shows that on increasing the prefactor, the extinction becomes less, due to the need for fewer larger-sized particles to conserve IWC. On the other hand, on decreasing the prefactor, to lower values, increases the extinction, due to the need for larger particles being required to conserve IWC. In this way, the transmission properties of the cloud can be varied, and from the measurements, the best optimized convolution of ensemble model weighting and shape of the PSD can be found.

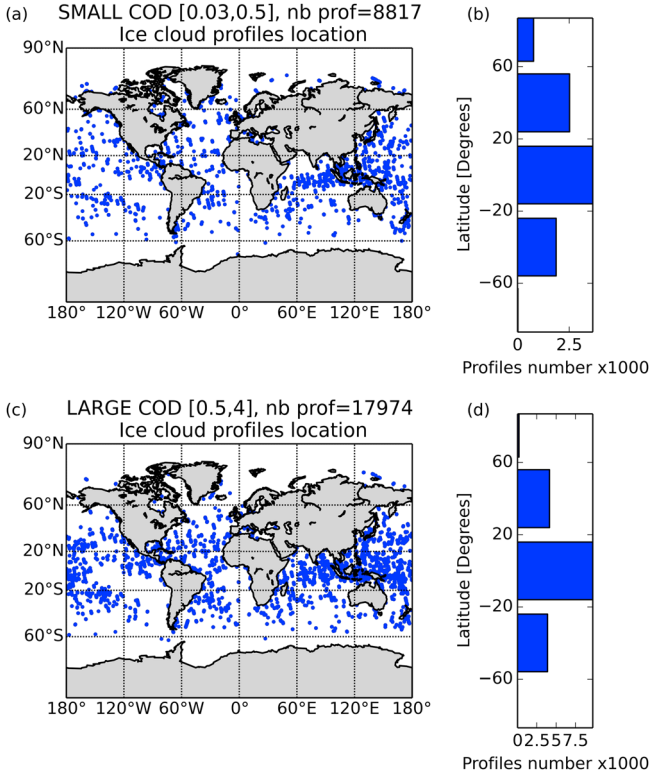

Figure 3. Global maps of selected ice cloud profiles for (a) small cloud optical depth and (c) large cloud optical depth for the two periods (22–28 February 2010 and 25–31 August 2010). (b and d) Zonal profiles number distributions are provided, respectively.

3. Selection of Ice Clouds

To evaluate the different RTTOV ice cloud parameterizations, we selected two different retrieval products of ice cloud profiles. The two products were retrieved from combined Lidar CALIOP (on board CALIPSO) and Radar CPR (on board CloudSat) instruments. The two products used in this paper are 2C-ICE [*Deng et al.*, 2010] and DARDAR [*Delanoë and Hogan*, 2010]. The two products provide information on the IWC and D_{eff} profiles, as well as the visible cloud optical depth (COD). The main differences between 2C-ICE and DARDAR are the vertical resolution of the product (CPR vertical resolution for 2C-ICE and CALIOP vertical resolution for DARDAR) and different assumptions for multiple scattering, lidar backscatter to extinction ratio, and parameterizations of radar and lidar signals [*Deng et al.*, 2013].

We selected the ice cloud profiles from 2 weeks (one in February and one in August 2010) of 2C-ICE and DARDAR product databases by using the DARDAR cloud mask product [*Delanoë and Hogan*, 2010]. The DARDAR cloud mask product was found to be better at removing aerosol-contaminated profiles than the CloudSat mask product. We also selected only profiles over oceans, to reduce potential land surface emissivity errors in our simulations, and when the pressures of the ice cloud layers were between 440 hPa (for the lowest layer) and 50 hPa (for the highest layer). We finally separated the selection into two groups of optical depth, one for COD between 0.03 and 0.5 (named small COD) and one for COD between 0.5 and 4 (named large COD).

Figures 3a and 3c represent the global location of ice cloud profiles for small and large CODs, respectively. The total number of profiles is 8817 profiles for small COD and 17,974 profiles for large COD. The zonal number of the profile distribution is shown in Figures 3b and 3d for each of the COD classifications, respectively. We separated the latitudes into the following five areas: High-Latitude North (90°N–60°N), Midlatitude North (60°N–20°N), Tropical Latitudes (20°N–20°S), Midlatitude South (20°S–60°S), and High-Latitude South (HLS) [60°S–90°S]. Most of the profiles are located in the tropics (with 41.2% and 54.2% of the total number of profiles for small and large CODs, respectively), and the profile distribution decreases toward the higher latitudes. For both COD classifications, there are significantly fewer profiles located at high latitudes (9% and 1.1% for small and large CODs, respectively). Figures 4a–4d show the mean and standard deviation profiles of IWC and D_{eff}, calculated from 2C-ICE (blue) and DARDAR (red). Figures 4a and 4b show the IWC and D_{eff} profiles for small COD, respectively, while Figures 4c and 4d show the same but for large COD. DARDAR generally retrieves more IWC and larger D_{eff} than 2C-ICE, except for D_{eff} in the highest layers. The difference between the two products mean and standard deviation profiles is more important for small COD, especially for IWC in the upper layers of ice clouds (see Figure 4a), above about 300 hPa.

4. Results

We compared the RTTOV TOA-simulated BT with TOA-observed BT, as measured by the IIR instrument on board CALIPSO in three channels. The response function of each of the IIR channels is centered on 8.65 μm

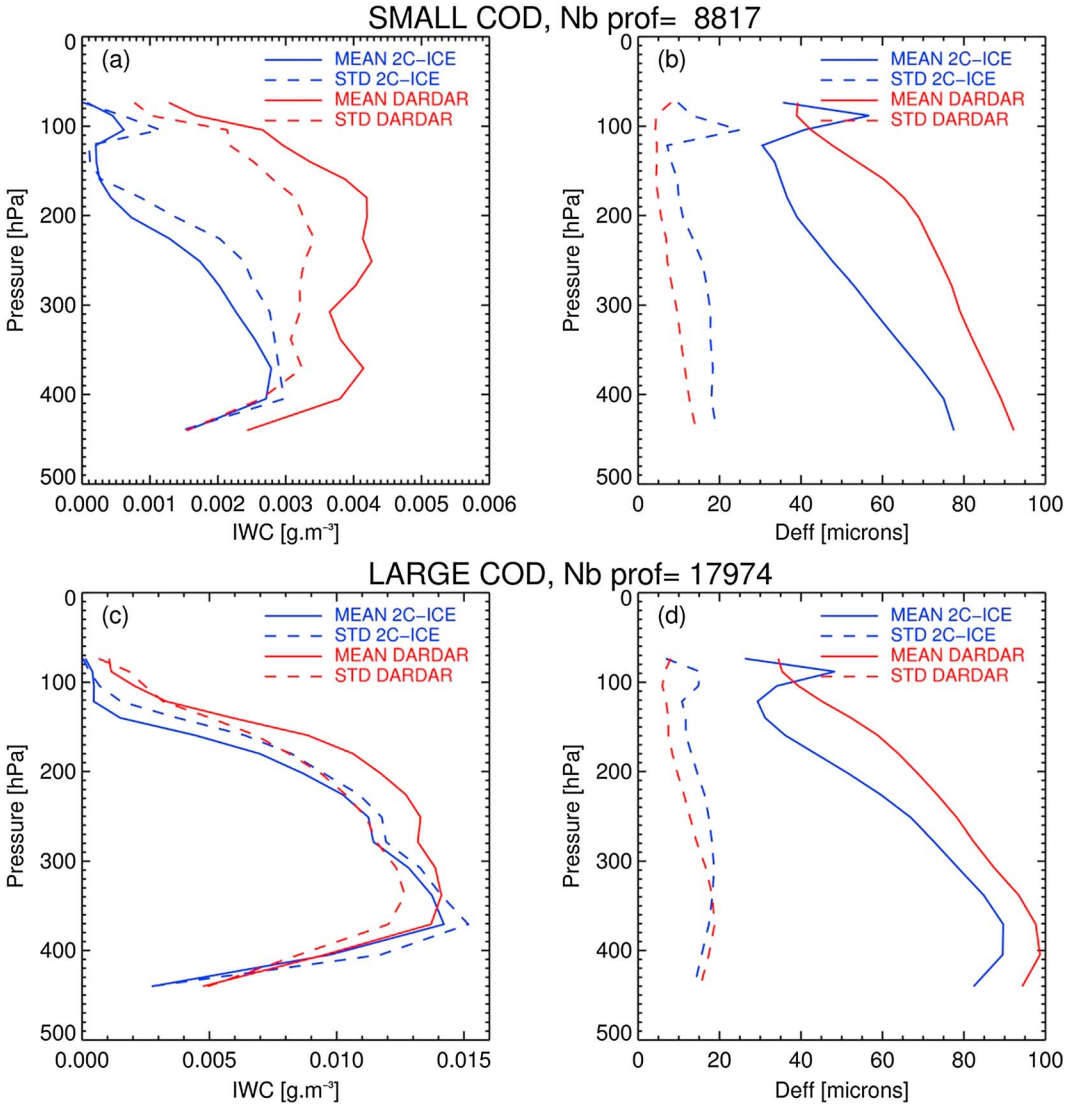

Figure 4. Mean and standard deviation profiles of (a) IWC and (b) D_{eff} from selected 2C-ICE profiles (in blue) and from selected DARDAR profiles (in red) for small COD. Mean and standard deviation profiles of (c) IWC and (d) D_{eff} for large COD, respectively.

(1156 cm^{-1}), 10.6 μm (943 cm^{-1}), and 12.05 μm (830 cm^{-1}). The absolute accuracy of the IIR channels is considered to be better than 1 K [*Corlay et al.*, 2000]. For all RTTOV simulations, we assume a cloud fraction of unity in any cloud layer. This assumption is supported by the fine spatial resolution of IIR (~1 km). To complete the needed inputs for RTTOV, we used collocated European Centre for Medium-Range Weather Forecasts (ECMWF) meteorological profiles (for pressure, temperature, specific humidity, and ozone mixing ratio) and collocated ECMWF surface pressure and 2 m temperature (ECMWF-AUX CloudSat product). We finally used collocated skin temperature from the Operational Sea Surface Temperature and Sea Ice Analysis (OSTIA) product [*Donlon et al.*, 2011]. This product was chosen because it was better to simulate clear-sky IIR observations as compared with the ECMWF skin temperature product (not shown here for reasons of brevity), and it provides a mask of sea ice for ice cloud cases in the high latitudes. The accuracy of RTTOV simulations in cloud-free situations was estimated by selecting 6629 clear-sky profiles for 22 February 2010. The biases and standard deviations between IIR observations minus RTTOV simulations were found to be -0.35 ± 0.76 K, -0.13 ± 0.82 K, and -0.23 ± 0.83 K for channels 1, 2, and 3, respectively.

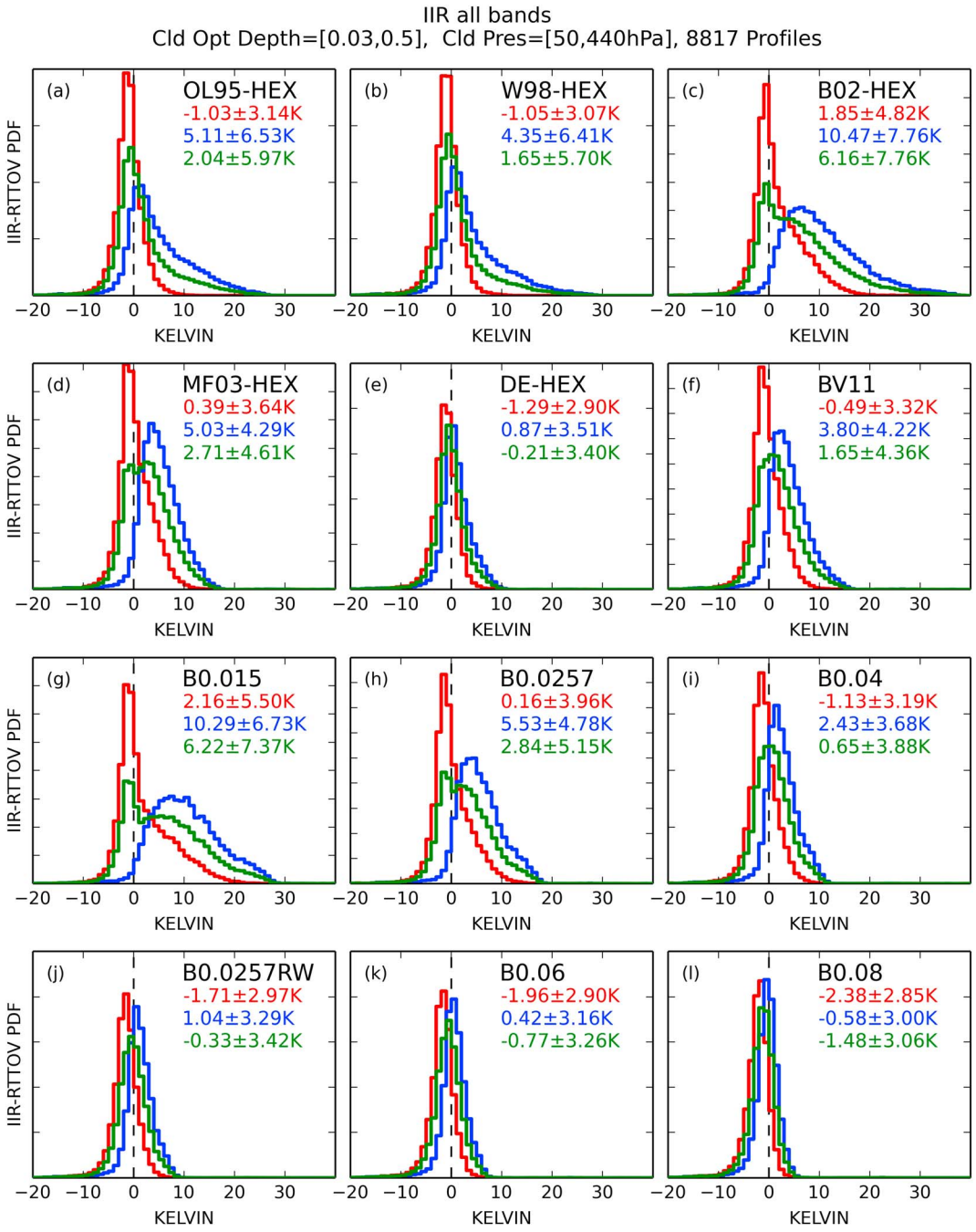

Figure 5. The normalized PDFs of IIR BT observations in all bands minus RTTOV BT simulations for the different ice cloud parameterizations, for small COD and from 2C-ICE (in red), from DARDAR (in blue), and from both 2C-ICE and DARDAR (in green) and the zero bias (black dashed line). Values of mean biases and standard deviations are provided in the legend. (a) OL95-HEX, (b) W98-HEX, (c) B02-HEX, and (d) MF03-HEX stand for the *Ou and Liou* [1995], *Wyser* [1998], *Boudala et al.* [2002], and *McFarquhar et al.* [2003] parameterizations, respectively. These parameterizations express the bulk optical properties as a function of the ice crystal effective diameter and IWC and/or temperature. (e) DE-HEX stands for the case where ice crystal effective diameter retrieved from satellite measurements was used together with hexagonal crystal optical parameterization. (f) BV11 stands for the current RTTOV version 11 parameterization of the SCSM model, and (g) B0.015, (h) B0.0257, (i) B0.04, (j) B0.0257RW, (k) B0.06, and (l) B0.08 stand for the parameterizations of the SCSM model with a prefactor of 0.015, 0.0257, 0.04, 0.0257 reweigthed, 0.06, and 0.08, respectively.

4.1. Global Results

Figures 5a–5l are IIR observations minus RTTOV simulations (O-B) represented as normalized probability density functions (PDFs) for small COD and for each of the parameterizations. The normalization is defined as the integral of the histogram summed to unity. The PDFs were calculated from the aggregation of the three O-B data sets corresponding to each of the IIR channels, leading to 3 times the number of selected profiles for each PDF. We simulated TOA BT by using 2C-ICE ice cloud profiles (in red), DARDAR ice cloud profiles (in blue), and both 2C-ICE and DARDAR (in green). The mean biases (μ) and standard deviations (σ) of the PDFs, derived from each of the parameterizations, shown in the panels, are given by

$$\mu = \frac{1}{3n}\sum_{i=1}^{3n}(O_i - B_i), \tag{6}$$

where n is the number of selected profiles and

$$\sigma = \sqrt{\frac{1}{3n}\sum_{i=1}^{3n}(O_i - \mu)^2}, \tag{7}$$

respectively.

Figures 5a–5f show the results for the current RTTOV-11 ice cloud parameterizations (excluding the aggregate shape for reasons given in section 1). The zero bias is shown by the vertical dashed lines. The results show that the PDFs are different when using 2C-ICE or DARDAR, except for the parameterization using the D_{eff} profiles as input (DE-HEX), see Figure 5e. With 2C-ICE ice cloud profile inputs (in red), RTTOV simulations are overestimated for OL95-HEX (Figure 5a), W98-HEX (Figure 5b), DE-HEX (Figure 5e), and BV11 (Figure 5f), with negative biases between -0.49 K and -1.29 K. RTTOV simulations are underestimated for B02-HEX (Figure 5c) and MF03-HEX (Figure 5d), with positive biases of 1.85 K and 0.39 K, respectively. With DARDAR ice cloud profiles (in blue), RTTOV simulations are more underestimated for most of the parameterizations (with positive biases between 3.8 K and 10.47 K), except for DE-HEX (Figure 5e), which has a bias of 0.87 K. Standard deviations (SDs) are also larger with DARDAR inputs. These results confirm the mean ice cloud profiles shown in Figure 4a, where the mean and standard deviation IWC profiles for small COD from DARDAR are greater than those from the 2C-ICE product, leading to lower BT simulations. Similarly, the lower difference between the DARDAR and 2C-ICE mean D_{eff} profiles (Figure 4b) is also obtained in the O-B PDF (see Figure 5e). These results also show that the comparison is very sensitive to the products of ice water content profiles used as inputs for RTTOV. To reduce this dependence on the ice cloud product, we aggregated TOA simulations from both products into the same data set. In the plot of Figure 5, the green lines represent the PDFs, when combining both products. The values of the mean biases and standard deviations are given in the legends. When combining 2C-ICE and DARDAR, and for most of the parameterizations, the O-B overestimation from 2C-ICE (due to lower IWC inputs) is cancelled out with the O-B underestimation from DARDAR IWC inputs. Figure 5e shows that the DE-HEX parameterization gave the lowest mean bias of -0.21 K with a SD of 3.4 K out of all current RTTOV parameterizations. However, this model was shown by *Baran and Francis* [2004] not to be a suitable model to use for the simultaneous simulation of high-resolution solar and infrared radiances measured from above and below the cirrus. Furthermore, the PSDs on which the DE-HEX parameterization is based were highly likely to have been affected by ice crystal shattering. This means that the overestimation of the occurrence of small ice crystals when convolved with the geometry of the hexagonal column could lead to a cancellation of error. Excluding the DE-HEX parameterization for the reasons given above means that the best agreement is found with the BV11 parameterization with $\mu = 1.65$ K and $\sigma = 4.36$ K (Figure 5f).

We experimented with further parameterizations to minimize O-B differences, to see if an optimal combination of PSD shape and optical properties could be found. This was achieved by modifying the SCSM database with the change of the mass-dimensional prefactor, as previously described in section 2. The effect of increasing the prefactor is (1) to change the mean bias from 6.22 K (for $a = 0.015$; Figure 5g) to -1.48 K (for $a = 0.08$; Figure 5i) and (2) to reduce the standard deviation from 7.37 K to 3.06 K, respectively. The best compromise is found for B0.0257RW, which represents the reweighted ensemble model, made to be consistent with the most current microphysics (Figure 5j). Using this parameterization, we found that $\mu = -0.33$ K and $\sigma = 3.42$ K. It is interesting to note here that the unweighted ensemble model results, assuming a prefactor of 0.0257 (Figure 5h), gives a combined $\mu = 2.84$ K and combined

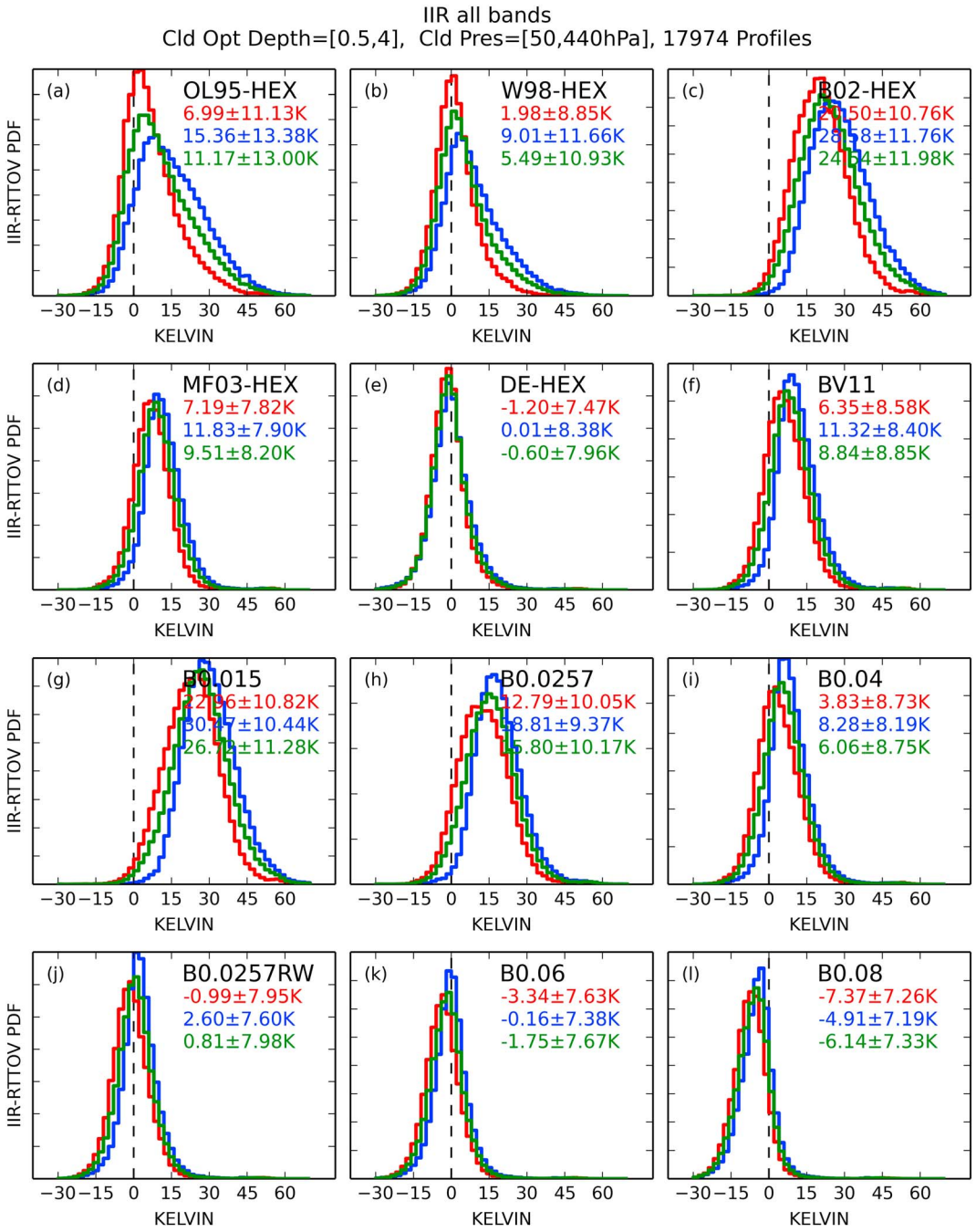

Figure 6. (a–l) Same as Figure 5 for large COD.

$\sigma = 5.15$ K, which means that, for small COD, the model was too biased toward the hexagonal ice column. The reason for this bias toward the hexagonal ice column is because it has been assigned to the first interval of the six equally divided intervals of the PSD, and it is over the first interval that the ice crystal number concentration is a maximum, which when convolved with the broader PSD (as can be seen from Figure 2), biased the simulated cloud BT's to colder temperatures.

Figures 6a–6l show the same comparison but for large COD. As compared to small COD, the differences between the distributions when using DARDAR or 2C-ICE is less important; however, standard deviations are much larger. These results confirm also the mean ice cloud profiles shown in Figures 4c and 4d, where the differences were found to be less between DARDAR and 2C-ICE IWC. When combining DARDAR and

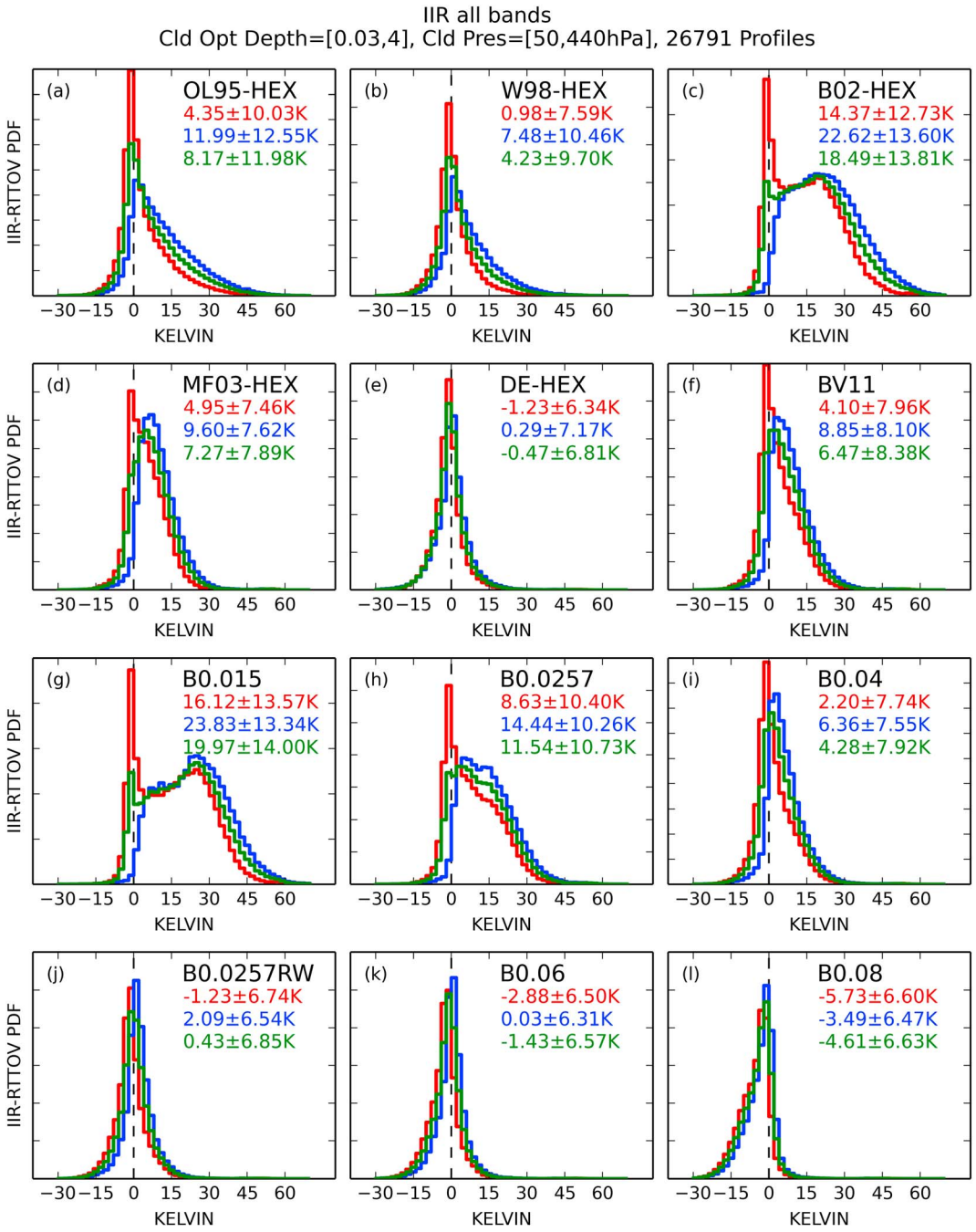

Figure 7. (a–l) Same as Figure 5 for all COD.

2C-ICE, the best agreement for the current RTTOV-11 ice cloud parameterizations (Figures 6a–6f) is again DE-HEX (Figure 6e) with $\mu = -0.6$ K and $\sigma = 7.96$ K (with caveats regarding previous comments about consistency and PSDs). If D_{eff} is not inputted, the second best agreement is found for the W98-HEX parameterization, with $\mu = 5.49$ K and $\sigma = 10.93$ K (Figure 6b). The same caveats apply to this parameterization with regard to geometry and the PSDs being affected by ice crystal shattering. By experimenting with the prefactor of the mass-dimensional relationship applied to the SCSM database, we can again improve the correlation with the same effect as for small COD, when increasing the prefactor and reweighting the ensemble model. For large COD, the best compromise is also found for B0.0257RW (Figure 6j), with $\mu = 0.81$ K and $\sigma = 7.98$ K, which is consistent with the results found for small COD.

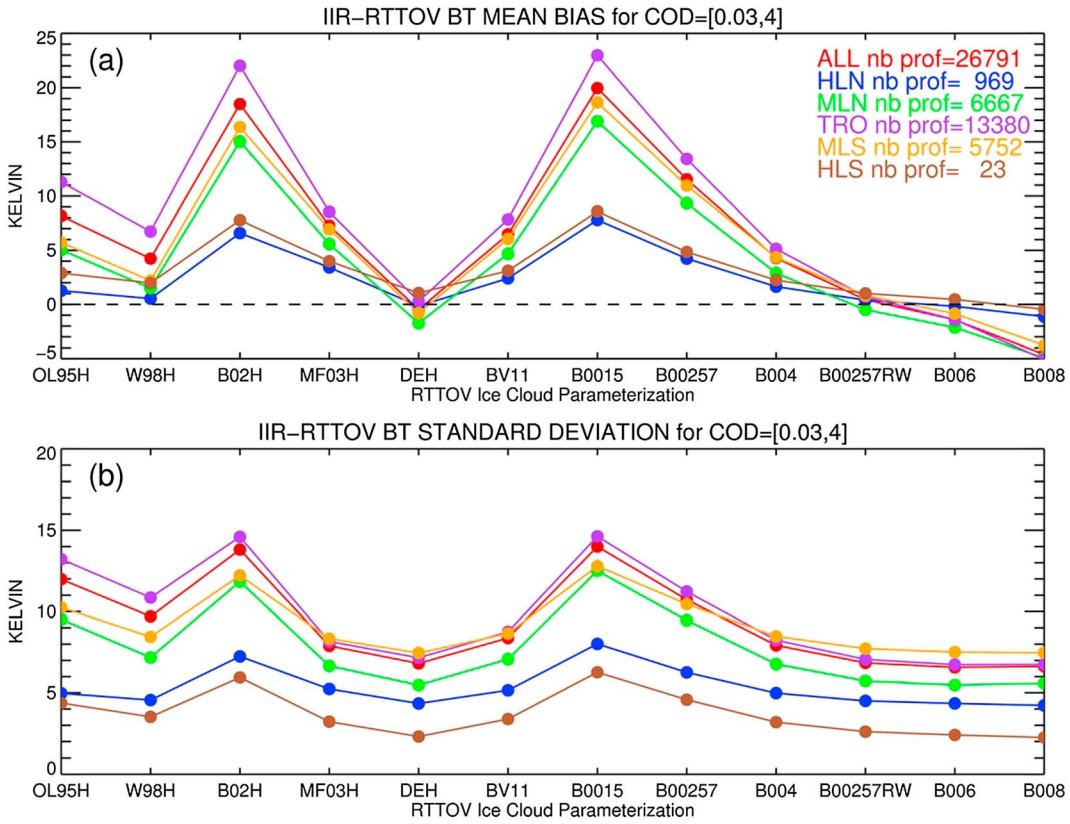

Figure 8. IIR BT observations minus RTTOV simulations (a) mean bias and (b) standard deviation versus RTTOV ice cloud parameterization from all COD profiles in all zonal areas (in red), in High-Latitude North (blue), in Midlatitude North (green), in Tropical Latitudes (purple), in Midlatitude South (orange), and in High-Latitude South (brown). The number of profiles for each area is given in Figure 8a legend.

Finally, we evaluated the comparison when adding the two COD groups to find out which one of the current RTTOV-11 parameterizations provides the best agreement. The results are depicted in Figures 7a–7l. The DE-HEX parameterization with $\mu = -0.47$ K and $\sigma = 6.81$ K (Figure 7e) is still the best of the current RTTOV-11 ice cloud parameterizations, and the W98-HEX parameterization with $\mu = 4.23$ K and $\sigma = 9.70$ K (Figure 7b), when D_{eff} is not inputted. Again, the previously stated caveats apply to these parameterizations.

The impact of changing the transmission properties of the SCSM, by increasing the prefactor in the mass-dimensional relationship to change the shape of the PSD, is also shown in Figure 7. The combined results show that the effect is to move the mean bias from underestimation to overestimation of the RTTOV BT simulations and to systematically reduce the standard deviation. Consistent with the results found for small and large CODs, the combined results show that the B0.0257RW parameterization provides the best agreement with the observations, with $\mu = 0.43$ K and $\sigma = 6.85$ K (Figure 7j). The remaining rather high value of the standard deviation may have different sources, as the uncertainties from IWC products or the error due to the RTTOV scattering approximation. As a comparison, other fast RTMs have shown similar standard deviations when comparing infrared observations and simulations in ice cloud situations [*Chen et al.*, 2008]. The results show that the B0.0257RW parameterization is closest to the current RTTOV-11 DE-HEX parameterization (Figure 7e). However, the B0.0257RW parameterization is the most consistent with current cirrus microphysics observations, in terms of PSDs, mass-dimensional relationships, and does not include significant biases in the small ice mode of the PSD due to ice crystal shattering. Moreover, simulations with this optimized parameterization are statistically very close to the simulations with the parameterization, when D_{eff} profile is inputted, and are statistically better than simulations with the other current RTTOV-11 ice cloud parameterizations. This section has shown that given a best-estimated PSD, from the latest observations of the mass-dimensional relationship [*Cotton et al.*, 2013], the ensemble model can be reweighted to find the

best optimal fit to the measurements. In principle, this can be applied to any shape of the PSD while maintaining microphysical consistency.

4.2. Zonal Results

We next studied whether the parameterizations have any zonal dependence. The results of this analysis are shown in Figure 8, which show the mean bias (Figure 8a) and standard deviation (Figure 8b) values for each of the parameterizations. As for Figure 7, the two groups of COD and all IIR channels were combined. The different colors shown in Figure 8 represent the different zonal areas, and the number of profiles in each zonal area defined in section 3 is given in the legend. The red line corresponds to values from Figure 7. The results found at the global scale can be applied for all zonal areas, even for HLS where very few profiles were selected. From Figure 8, it can be seen that the least zonally biased parameterization is B0.0257RW. Therefore, whatever the zone, the optimized B0.0257RW parameterization better simulates the IIR TOA BT in the presence of ice clouds.

5. Conclusions

A Self-Consistent Scattering Model (SCSM) database of ice cloud optical properties in the thermal infrared has been parameterized and implemented into RTTOV-11. This new parameterization allows a direct estimation of the cloud optical properties from the IWC and the ambient temperature T profiles, avoiding the choice of an effective diameter relationship and the shape of ice crystals. To evaluate this new parameterization, with other RTTOV ice cloud parameterizations, we selected a data set of ice cloud profiles from 2C-ICE and DARDAR products. The comparison of simulated TOA brightness temperatures against collocated IIR observations showed that the best parameterizations to apply are DE-HEX and B0.0257RW, where, in the case of DE-HEX, the effective size profile of ice cloud has to be provided as input to RTTOV. We point out here that the B0.0257RW parameterization is directly related to the NWP or climate model prognostic variable IWC, whereas D_{eff} has to be diagnosed, usually within the radiation scheme of NWP or climate models, and this diagnosis depends on empirical fits between D_{eff} and environmental temperature and/or IWC. Moreover, the single hexagonal column cannot be applied across the electromagnetic spectrum as demonstrated by *Baran and Francis* [2004]. Furthermore, the older RTTOV-11 parameterizations are based on PSDs which are highly likely to have been affected by ice crystal shattering, thereby resulting in underestimated D_{eff} values [*Mitchell et al.*, 2011]. Nevertheless, for all parameterizations, the mean biases between simulated and observed brightness temperatures are still up to a few kelvins. A recent paper by *Fauchez et al.* [2014] has shown that cirrus heterogeneities can impact simulations of brightness temperatures in the terrestrial window region by several kelvins when compared against RTM assuming plane-parallel and homogeneous layers. Therefore, the remaining biases shown in this paper could be due to 3-D cloud effects, which should be taken into account in future simulations through some form of parameterization.

To obtain the B0.0257RW parameterization, which is fundamentally based on the SCSM database, we used the selected data set of ice cloud profiles to minimize the bias between simulations and observations. We demonstrated that by modifying the prefactor of the mass-dimensional law of the PSD, to match the *Cotton et al.*'s [2013] observationally derived mass-dimensional relationship, we could reduce the bias from 6.47 K to 0.43 K and the standard deviation from 8.38 K to 6.85 K for the complete range of visible COD used in this study. Indeed, the B0.0257RW parameterization was demonstrated to be the least zonally biased out of all the current RTTOV-11 parameterizations. As a result of this finding, in the next version of RTTOV, we will replace the current SCSM parameterization (BV11) with the optimized SCSM database parameterization (B0.0257RW). This parameterization can also be applied to any other fast radiative transfer model [see for example *Havemann et al.*, 2009; *Thelen et al.*, 2012]. This parameterization may also be applied to general circulation models, since the SCSM database has already been parameterized in a simplistic manner and tested in the Met Office Unified Model Global Atmosphere configuration 5.0 setup [*Baran et al.*, 2014b]. In future studies, the RTTOV parameterizations will be tested at wavelengths ranging from the visible to the near infrared.

Acknowledgments

This study was accomplished in the frame of the NWP-SAF project funded by EUMETSAT and was also supported by the French national program LEFE/INSU. We gratefully acknowledge the NASA CloudSat project for providing 2C-ICE and CloudSat products (http://www.cloudsat.cira.colostate.edu/data-products). We also thank the ICARE data and service center for providing the DARDAR cloud and mask products (http://www.icare.univ-lille1.fr/drupal/projects/dardar) and the Met Office for maintaining and providing the OSTIA products in the frame of the MyOcean European Project (http://ghrsst-pp.metoffice.com/pages/latest_analysis/ostia.html). The optical properties on which the optimized SCSM database parameterization is based are freely available upon request to Anthony Baran. We would like also to thank anonymous reviewers for helping to improve the manuscript.

References

Baran, A. J., and P. N. Francis (2004), On the radiative properties of cirrus cloud at solar and thermal wavelengths: A test of model consistency using high-resolution airborne radiance measurements, *Q. J. R. Meteorol. Soc.*, *130*, 763–778.

Baran, A. J., and L.-C. Labonnote (2007), A self-consistent scattering model for cirrus. I: The solar region, *Q. J. R. Meteorol. Soc.*, *133*, 1899–1912.

Baran, A. J., P. N. Francis, L.-C. Labonnote, and M. Doutriaux-Boucher (2001), A scattering phase function for ice cloud: Tests of applicability using aircraft and satellite multi-angle multi-wavelength radiance measurements of cirrus, *Q. J. R. Meteorol. Soc.*, *127*, 2395–2416.

Baran, A. J., P. J. Connolly, A. J. Heymsfield, and A. Bansemer (2011a), Using in situ estimates of ice water content, volume extinction coefficient, and the total solar optical depth obtained during the tropical ACTIVE campaign to test an ensemble model of cirrus ice crystals, *Q. J. R. Meteorol. Soc.*, *137*, 199–218, doi:10.1002/qj.731.

Baran, A. J., A. Bodas-Salcedo, R. Cotton, and C. Lee (2011b), Simulating the equivalent radar reflectivity of cirrus at 94 GHz using an ensemble model of cirrus ice crystals: A test of the Met Office global numerical weather prediction model, *Q. J. R. Meteorol. Soc.*, *137*, 1547–1560.

Baran, A. J., R. Cotton, K. Furtado, S. Havemann, L.-C. Labonnote, F. Marenco, A. Smith, and J.-C. Thelen (2014a), A self-consistent scattering model for cirrus. II: The high and low frequencies, *Q. J. R. Meteorol. Soc.*, doi:10.1002/qj.2193.

Baran, A. J., P. Hill, K. Furtado, P. Field, and J. Manners (2014b), A coupled cloud physics–radiation parameterization of the bulk optical properties of cirrus and its impact on the Met Office Unified Model Global Atmosphere 5.0 configuration, *J. Clim.*, *27*, 7725–7752, doi:10.1175/JCLI-D-13-00700.1.

Bauer, P., et al. (2011), Satellite cloud and precipitation assimilation at operational NWP centres, *Q. J. R. Meteorol. Soc.*, *137*, 1934–1951, doi:10.1002/qj.905.

Baum, B. A., P. Yang, S. Nasiri, A. K. Heidinger, A. Heymsfield, and J. Li (2007), Bulk scattering properties for the remote sensing of ice clouds. Part III: High-resolution spectral models from 100 to 3250 cm^{-1}, *J. Appl. Meteorol. Climatol.*, *46*, 423–434, doi:10.1175/JAM2473.1.

Baum, B. A., P. Yang, A. J. Heymsfield, A. Bansemer, A. Merrelli, C. Schmitt, and C. Wang (2014), Ice cloud bulk single-scattering property models with the full phase matrix at wavelengths from 0.2 to 100 μm, *J. Quant. Spectrosc. Radiat. Transfer*, *146*, 123–139, doi:10.1016/j.jqsrt.2014.02.029.

Boudala, F. S., G. A. Isaac, Q. Fu, and S. G. Cober (2002), Parameterization of effective ice particle size for high-latitude clouds, *Int. J. Clim.*, *22*, 1267–1284.

Chen, Y., F. Weng, Y. Han, and Q. Liu (2008), Validation of the community radiative transfer model by using CloudSat data, *J. Geophys. Res.*, *113*, D00A03, doi:10.1029/2007JD009561.

Chou, M. D., K. T. Lee, S. C. Tsay, and Q. Fu (1999), Parameterization for cloud longwave scattering for use in atmospheric models, *J. Clim.*, *12*, 159–169.

Corlay, G., M.-C. Arnolfo, T. Bret-Dibat, A. Lifferman, and J. Pelon (2000), The infrared imaging radiometer for PICASSOCENA. [Available at http://smsc.cnes.fr/CALIPSO/IIR_ICSO00_S2-06.pdf.]

Cotton, R. J., P. R. Field, Z. Ulanowski, P. H. Kaye, E. Hirst, R. S. Greenaway, I. Crawford, J. Crosier, and J. Dorsey (2013), The effective density of small ice particles obtained from in situ aircraft observations of mid-latitude cirrus, *Q. J. R. Meteorol. Soc.*, *139*, 1923–1934.

Delanoë, J., and R. J. Hogan (2010), Combined CloudSat-CALIPSO-MODIS retrievals of the properties of ice clouds, *J. Geophys. Res.*, *115*, D00H29, doi:10.1029/2009JD012346.

Deng, M., G. G. Mace, Z. Wang, and H. Okamoto (2010), Tropical Composition, Cloud and Climate Coupling Experiment validation for cirrus cloud profiling retrieval using CloudSat radar and CALIPSO lidar, *J. Geophys. Res.*, *115*, D00J15, doi:10.1029/2009JD013104.

Deng, M., G. G. Mace, Z. Wang, and R. P. Lawson (2013), Evaluation of several A-Train ice cloud retrieval products with in situ measurements collected during the SPARTICUS campaign, *J. Appl. Meteorol. Climatol.*, *52*, 1014–1030, doi:10.1175/JAMC-D-12-054.1.

Donlon, C. J., M. Martin, J. D. Stark, J. Roberts-Jones, E. Fiedler, and W. Wimmer (2011), The Operational Sea Surface Temperature and Sea Ice Analysis (OSTIA), *Remote Sens. Environ.*, doi:10.1016/j.rse.2010.10.017.

Errico, R. M., G. Ohring, F. Weng, P. Bauer, B. Ferrier, J.-F. Mahfouf, and J. Turk (2007), Assimilation of satellite cloud and precipitation observations in numerical weather prediction models: Introduction to the JAS special collection, *J. Atmos. Sci.*, *64*, 3737–3741.

Faijan, F., L. Lavanant, and F. Rabier (2012), Towards the use of cloud microphysical properties to simulate IASI spectra in an operational context, *J. Geophys. Res.*, *117*, D22205, doi:10.1029/2012JD017962.

Fauchez, T., C. Cornet, F. Szczap, P. Dubuisson, and T. Rosambert (2014), Impact of cirrus clouds heterogeneities on top-of-atmosphere thermal infrared radiation, *Atmos. Chem. Phys.*, *14*, 5599–5615, doi:10.5194/acp-14-5599-2014.

Field, P. R., R. Wood, P. R. A. Brown, P. H. Kaye, E. Hirst, R. Greenaway, and J. A. Smith (2003), Ice particle interarrival times measured with a fast FSSP, *J. Atmos. Oceanic Technol.*, *20*, 249–261, doi:10.1175/1520-0426(2003)020<0249:IPITMW>2.0.CO;2.

Field, P. R., A. J. Heymsfield, and A. Bansemer (2007), Snow size distribution parameterization for midlatitude and tropical ice clouds, *J. Atmos. Sci.*, *64*, 4346–4365.

Field, P. R., R. J. Cotton, K. McBeath, A. P. Lock, S. Webster, and R. P. Allan (2014), Improving a convection-permitting model simulation of a cold air outbreak, *Q. J. R. Meteorol. Soc.*, *140*, 124–138, doi:10.1002/qj.2116.

Garnier, A., J. Pelon, P. Dubuisson, M. Faivre, O. Chomette, N. Pascal, and D. P. Kratz (2012), Retrieval of cloud properties using CALIPSO Imaging Infrared Radiometer. Part I: Effective emissivity and optical depth, *J. Appl. Meteorol. Climatol.*, *51*, 1407–1425, doi:10.1175/JAMC-D-11-0220.1.

Guidard, V., N. Fourrié, P. Brousseau, and F. Rabier (2011), Impact of IASI assimilation at global and convective scales and challenges for the assimilation of cloudy scenes, *Q. J. R. Meteorol. Soc.*, *137*, 1975–1987, doi:10.1002/qj.928.

Havemann, S., J.-C. Thelen, J. P. Taylor, and A. Keil (2009), The Havemann–Taylor fast radiative transfer code: Exact fast radiative transfer for scattering atmospheres using principal components (PCs), in *Proceedings of the International Radiation Symposium (IRC/IAMAS)*, AIP Conf. Proc., vol. 1100, pp. 38–40, doi:10.1063/1.3117000.

Hess, M., and M. Wiegner (1994), COP: A data library of optical properties of hexagonal ice crystals, *Appl. Opt.*, *33*, 7740–7746.

Hess, M., P. Koepke, and I. Schult (1998), Optical properties of aerosols and clouds: The software package OPAC, *Bull. Am. Meteorol. Soc.*, *79*, 831–844, doi:10.1175/1520-0477(1998)079<0831:OPOAAC>2.0.CO;2.

Korolev, A. V., E. F. Emery, J. W. Strapp, S. G. Cober, G. A. Isaac, M. Wasey, and D. Marcotte (2011), Small ice particles in tropospheric clouds: Fact or artifact? Airborne icing instrumentation evaluation experiment, *Bull. Am. Meteorol. Soc.*, *92*, 967–973, doi:10.1175/2010BAMS3141.1.

Martinet, P., N. Fourrié, V. Guidard, F. Rabier, T. Montmerle, and P. Brunel (2013a), Towards the use of microphysical variables for the assimilation of cloud-affected infrared radiances, *Q. J. R. Meteorol. Soc.*, *139*, 1402–1416, doi:10.1002/qj.2046.

Martinet, P., L. Lavanant, N. Fourrié, F. Rabier, and A. Gambacorta (2013b), Evaluation of a revised IASI channel selection for cloudy retrievals with a focus on the Mediterranean basin, *Q. J. R. Meteorol. Soc.*, doi:10.1002/qj.2239.

Matricardi, M. (2005), The inclusion of aerosols and clouds in RTIASI, the ECMWF fast radiative transfer model for the infrared atmospheric sounding interferometer, ECMWF Tech. Memo., 474.

Matricardi, M., F. Chevallier, G. Kelly, and J.-N. Thépaut (2004), An improved general fast radiative transfer model for the assimilation of radiance observations, *Q. J. R. Meteorol. Soc.*, *130*, 153–173, doi:10.1256/qj.02.181.

McFarquhar, G. M., S. Iacobellis, and R. C. J. Somerville (2003), SCM simulations of tropical ice clouds using observationally based parameterizations of microphysics, *J. Clim.*, *16*, 1643–1664.

McNally, A. P. (2009), The direct assimilation of cloud-affected satellite infrared radiances in the ECMWF 4D-Var, *Q. J. R. Meteorol. Soc.*, *135*, 1214–1229, doi:10.1002/qj.426.

Mitchell, D. L., R. P. Lawson, and B. Baker (2011), Understanding effective diameter and its application to terrestrial radiation in ice clouds, *Atmos. Chem. Phys.*, *11*, 3417–3429, doi:10.5194/acp-11-3417-2011.

Okamoto, K., A. P. McNally, and W. Bell (2013), Progress towards the assimilation of all-sky infrared radiances: An evaluation of cloud effects, *Q. J. R. Meteorol. Soc.*, doi:10.1002/qj.2242.

Ou, S. C., and K. N. Liou (1995), Ice microphysics and climatic temperature feedback, *Atmos. Res.*, *35*, 127–138.

Pavelin, E. G., S. J. English, and J. R. Eyre (2008), The assimilation of cloud-affected infrared satellite radiances for numerical weather prediction, *Q. J. R. Meteorol. Soc.*, *134*, 737–749.

Saunders, R., M. Matricardi, and P. Brunel (1999), A improved fast radiative transfer model for assimilation of satellite radiance observations, *Q. J. R. Meteorol. Soc.*, *125*, 1407–1425.

Saunders, R., M. Matricardi, A. Geer, P. Rayer, O. Embury, and C. Merchant (2009), RTTOV-9 Science and Validation Report. [Available at https://nwpsaf.eu/deliverables/rtm/rttov9_files/rttov9_svr.pdf.]

Saunders, R., J. Hocking, P. Rayer, M. Matricardi, A. Geer, and N. Bormann (2012), RTTOV-10 Science and Validation Report. [Available at https://nwpsaf.eu/deliverables/rtm/docs_rttov10/rttov10_svr_1.11.pdf.]

Saunders, R., J. Hocking, D. Rundle, P. Rayer, M. Matricardi, A. Geer, C. Lupu, P. Brunel, and J. Vidot (2013), RTTOV-11 Science and Validation Report. [Available at https://nwpsaf.eu/deliverables/rtm/docs_rttov11/rttov11_svr.pdf.]

Stengel, M., M. Lindskog, P. Undén, N. Gustafsson, and R. Bennartz (2010), An extended observation operator in HIRLAM 4D-VAR for the assimilation of cloud-affected satellite radiances, *Q. J. R. Meteorol. Soc.*, *136*, 1064–1074, doi:10.1002/qj.621.

Stengel, M., M. Lindskog, P. Undén, and N. Gustafsson (2013), The impact of cloud-affected IR radiances on forecast accuracy of a limited-area NWP model, *Q. J. R. Meteorol. Soc.*, *139*, 2081–2096, doi:10.1002/qj.2102.

Stephens, G. L., et al. (2002), The CloudSat mission and the A-Train, *Bull. Am. Meteorol. Soc.*, *83*, 1771–1790, doi:10.1175/BAMS-83-12-1771.

Thelen, J.-C., S. Havemann, and J. P. Taylor (2012), Atmospheric correction of shortwave hyperspectral imagery using a fast, full-scattering 1DVar retrieval scheme, in *Algorithms and Technologies for Multispectral, Hyperspectral, and Ultraspectral Imagery XVIII*, Proc. SPIE, 839010, edited by S. S. Shen and P. E. Lewis, doi:10.1117/12.918012.

Vidot, J., P. Brunel, and A. J. Baran (2013), A new ice cloud optical properties database in RTTOV for IASI, Third International IASI Conference, Hyères, France, 4–8, poster 40, 4–8 February. [Available at http://smsc.cnes.fr/IASI/PDF/conf3/posters/40_Vidot_J.pdf.]

Winker, D. M., M. A. Vaughan, A. Omar, Y. Hu, K. A. Powell, Z. Liu, W. H. Hunt, and S. A. Young (2009), Overview of the CALIPSO mission and CALIOP data processing algorithms, *J. Atmos. Oceanic Technol.*, *26*, 2310–2323, doi:10.1175/2009JTECHA1281.1.

Wyser, K. (1998), The effective radius in ice clouds, *J. Clim.*, *11*, 1793–1802.

Yang, P., B.-C. Gao, B. A. Baum, Y. X. Hu, W. J. Wiscombe, S.-C. Tsay, D. M. Winker, and S. L. Nasiri (2001), Radiative properties of cirrus clouds in the infrared (8–13 μm) spectral region, *J. Quant. Spectrosc. Radiat. Transfer*, *70*, 473–504, doi:10.1016/S0022-4073(01)00024-3.

Yang, P., H. Wei, H. Huang, B. Baum, Y. Hu, G. Kattawar, M. Mishchenko, and Q. Fu (2005), Scattering and absorption property database for nonspherical ice particles in the near- through far-infrared spectral region, *Appl. Opt.*, *44*, 5512–5523.

Yang, P., L. Bi, B. A. Baum, K.-N. Liou, G. Kattawar, M. Mishchenko, and B. Cole (2013), Spectrally consistent scattering, absorption, and polarization properties of atmospheric ice crystals at wavelengths from 0.2 μm to 100 μm, *J. Atmos. Sci.*, *70*, 330–347.